Surface & Coatings Technology 239 (2014) 191–199

Contents lists available at ScienceDirect

Surface & Coatings Technology

journal homepage: www.elsevier.com/locate/surfcoat

Interface melding in cold spray titanium particle impact

Peter C. King [a,*], Christian Busch [b], Teresa Kittel-Sherri [c], Mahnaz Jahedi [a], Stefan Gulizia [a]

[a] CSIRO Materials Science and Engineering, Gate 5, Normanby Road, Clayton, VIC 3168, Australia
[b] Helmut Schmidt University, University of the Federal Armed Forces, Institute for Materials Technology, Hamburg, Germany
[c] CSIRO Process Science and Engineering, Gate 1, Normanby Road, Clayton, VIC 3168, Australia

ARTICLE INFO

Article history:
Received 9 September 2013
Accepted in revised form 18 November 2013
Available online 27 November 2013

Keywords:
Cold spray
Titanium
Bonding
Adiabatic shear
Focused ion beam

ABSTRACT

A focused ion beam (FIB) was used to characterize deformation and bonding behavior of titanium particles, cold sprayed onto a titanium surface. By milling away half of each particle a cross-section was obtained, revealing the particle–substrate interface. It was found that in some sections, voids lined the interface due to mismatch in particle- and substrate-surface topologies. In other places, the interface could not be discerned due to closure of the voids. It is shown that this effect was related to adiabatic shear instability, which caused violent jetting, ejection of molten material from the particle, and thermal softening of the interfacial layers. Deformation characteristics and variation in splat profiles due to microstructural influences, and the effect of particle size are also discussed.

1. Introduction

Cold spray is a process for the building up of coatings by high velocity impact of powder particles [1]. The particles, typically 1–50 μm in size, are accelerated within a supersonic gas stream towards a substrate surface. Unlike in other thermal spray processes, the material is not melted in-flight. Therefore, coatings may be deposited that are free from quenching stresses, oxidation and other thermal defects.

There have been several studies of cold sprayed titanium [2–9]. Titanium and its alloys exhibit high strength-to-weight ratios, oxidation resistance, corrosion resistance and biocompatibility which make them an attractive choice for demanding applications. By cold spray, titanium has a higher critical velocity for deposition than other, more ductile metals [8]. Nevertheless, a deposition efficiency (fraction of sprayed powder which remains in the deposit) of 100% is readily obtainable using relatively inexpensive N_2 as the accelerating gas [7]. Additive manufacture of titanium components by cold spray (spray forming) is also being actively pursued [3,4]. In order to achieve high strengths within cold sprayed Ti parts and coatings it is necessary to understand the mechanism of bonding between cold spray particles.

Bonding of cold spray particles comes about as a result of the plastic deformation that occurs upon impact. Owing to their small size, the deformation period (or contact time) of individual particles is generally less than 100 ns [10]. Deformation occurs at high strain rates (up to ~10^7 s^{-1}) under near-adiabatic conditions. Plastic strain is highly localized in a layer of material at the interface where intense shearing occurs. This interfacial shearing is manifest as thin, outward-moving 'jets'. In finite element models (FEM) of particle impact the velocity needed to induce adiabatic shear instability has been shown to correspond to the experimentally-determined critical velocity for deposition [11,12]. Thus, there appears to be a dependence of particle adhesion on the interfacial jets. Mechanistically, it has been proposed that the jetting action is violent enough to disrupt passive oxide films, allowing intimate contact of the metal surfaces and formation of metallic bonds across the interface [13,14].

FEM also shows that the temperature rise due to adiabatic plastic deformation within the interfacial jets generally approaches or may even reach melting point. The latter is supported by empirical observation of 'splashes', spheroidized ejecta [15,16] and other signs of melting. For instance, in bimetallic systems (e.g. when copper particles are sprayed onto aluminum) intermetallic compounds form at the interface due to melting [17–19].

Away from the interface within the bulk of the particle, strains are considerably lower and there is minimal temperature rise [11]. In other words, melting is an interfacial phenomenon only, and the vast bulk of the cold sprayed material remains well within the solid state.

A further, important outcome of FEM simulations is that when strains and temperatures are mapped over the particle–substrate interface, it is found that they are much greater in the peripheral zone (i.e. within the shear jets) than at the base (so-called south pole [11]) of the particle [11,17]. Thus if bonding is associated with adiabatic shearing, then only a fraction of the contact area may in fact be bonded. This has implications for the adhesion of cold sprayed coatings onto surfaces, as well as for the cohesive strength within the deposits themselves. Assadi et al. measured the bond strength copper coatings and obtained a value 20% of the ultimate tensile strength of copper. This

* Corresponding author. Tel.: +61 3 9545 2744.
E-mail addresses: Peter.King@csiro.au (P.C. King), Christian.Busch@hsu-hh.de (C. Busch), Terri.Kittel-Sherri@csiro.au (T. Kittel-Sherri), Mahnaz.Jahedi@csiro.au (M. Jahedi), Stefan.Gulizia@csiro.au (S. Gulizia).

0257-8972/$ – see front matter.
http://dx.doi.org/10.1016/j.surfcoat.2013.11.039

figure, they noted, was in good agreement with their modeling of 580 m/s Cu-on-Cu impact, in which only 15–25% of the interface was found to be subject to shear instability [11].

There is however, only a small body of experimental evidence that directly links bonding with the peripheral shear zones. It has been done by examination of rebound sites of metallic particles against rigid surfaces. When aluminum particles strike a ceramic surface [15] or when Al–Si particles impact mild steel [20], a thin, Al-rich layer is left behind due to a brief, adhesive interaction between the two bodies. The layer is generally ring shaped, due to this interaction occurring predominantly at the edges of the particle. In another study, the 'scrubbing' action of Ti particles' jets has been demonstrated by impact onto a gold-plated surface. Abrasive thinning or removal of the 30 nm Au film was found to occur, again in a ring-shaped pattern [21].

Although in the broader literature a number of different cold spray bonding scenarios have been investigated, the one with the broadest practical relevance is that of a particle impacting a surface composed of the same material, as it relates to the process of coating buildup. Therefore, in this study the impact of titanium particles onto a flat, polished titanium surface was investigated. While a cold sprayed surface is far from microscopically flat, the flat surface is nonetheless a simpler geometry which facilitates a more controlled study of particle deformation and bonding. Furthermore it is hoped that the obtained data will serve as a useful empirical base for computer models, which tend to focus on the spherical particle – on – flat surface geometry. Selected particles were milled with a focused ion beam (FIB) to make an exact cross-section. This revealed the total shape of the deformed particle and substrate. It also allowed close examination of the particle–substrate interface to determine the location at which bonding was more favorable.

2. Experimental methods

Gas atomized grade 2 titanium powder (TLS Technik, Bitterfeld, Germany) was chosen as the feedstock (Table 1). The particle size distribution was determined by laser measurement using a Malvern Mastersizer X (Malvern Instruments Ltd., Malvern, Worcestershire, UK). The median particle size (d_{50}) was found to be 21.89 μm, d_{10} = 12.12 μm, and d_{90} = 34.17 μm. The particle morphologies were approximately spherical (as seen in the SEM shown in Fig. 1) although from measurements of particle dimensions in two orthogonal directions a mean particle aspect ratio of 1.12 was calculated. Small 'satellite particles' attached to larger ones were relatively few.

The substrates were 11 mm-thick disks cut from round, 25.4 mm-diameter grade 2 titanium bar stock. An average grain size of 17.4 ± 0.8 μm was measured by optical image analysis. The flat surface of the disks was polished using progressively finer diamond suspensions with applied force limited to 10 N. The final polishing step was done with 0.25 μm colloidal silica.

Cold spray was performed with a CGT Kinetiks® 4000 system. N_2 carrier gas was accelerated through a CGT 24TC converging–diverging nozzle with circular cross-section. This nozzle had a diverging section length of 129 mm, throat diameter of 2.7 mm and an exit diameter of 6.6 mm. The chosen gas stagnation temperature and pressure were 600 °C and 3.0 MPa, respectively. The cold spray gun was held by an ABB IRB 2600 robot arm.

Titanium splats were deposited on the polished samples using a method that differed from the commonly used 'wipe test' [15,22]. In the wipe test, the nozzle is moved quickly past the sample to spatter particles in a line across the surface. This method suffers the following limitations.

- Due to divergence of the beam it is not possible to distinguish particles that arrived at the surface along a straight trajectory in the center of the beam, from those that were deposited slightly ahead or slightly behind.
- The temperature of the surface at the moment of impact of the particles cannot easily be measured or calculated.

Others [19] have used a mask between the gun and substrate which opens briefly, usually by moving the mask so that a slit comes momentarily in line with the particle jet. The problem of determining the particle position within the diverging beam is also solved by this approach.

In this study, the cold spray jet was moved onto the polished disk (at a nozzle standoff distance of 30 mm) and held there for 40 s to ensure that the substrate surface temperature had reached a steady state condition. The powder feed was then briefly turned on and then off. The nozzle was held in position for a further ~2 s, to allow any residual particles in the feed lines to exit through the nozzle, and then was moved away. A circular spot pattern resulted, with particles more concentrated in the center, and diminishing in frequency with distance, until no particles were found >5.5 mm from the center. This method was used to spray several disk samples. However upon inspection under a microscope, only two were chosen for further study on the basis of their

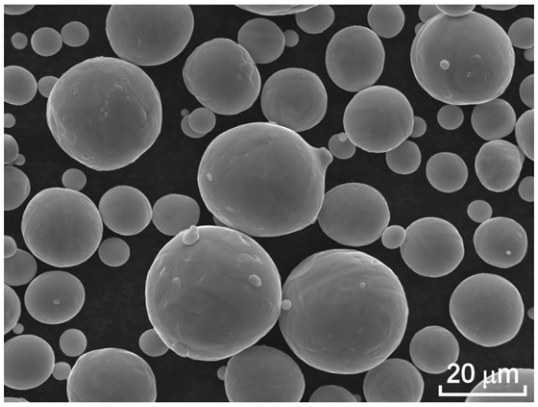

Fig. 1. Scanning electron micrograph of titanium powder feedstock.

Table 1
Titanium powder composition (from supplier, TLS, Germany).

	C	Fe	O	N	H	Zn	Ti
Element-%	0.004	0.03	0.18	0.008	0.001	<0.002	remainder

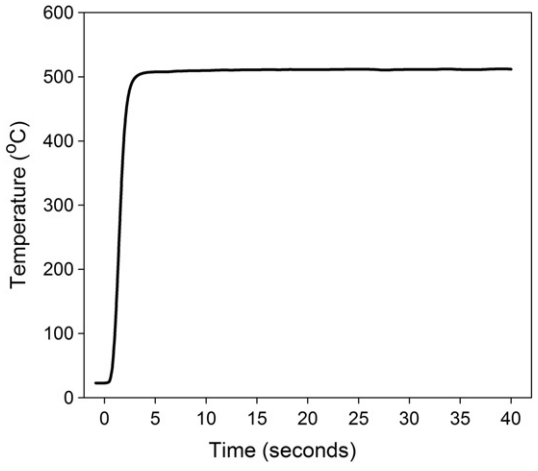

Fig. 2. Substrate surface temperature rise due to cold spray gas jet impingement.

having a low enough number of particles for the majority of particles to be non-contacting with their nearest neighbors.

In order to determine the extent of substrate heating due to the impinging gas jet and to verify that a steady state had been reached, a k-type thermocouple was clamped against the titanium surface and the cold spray test repeated without turning the particle feed on. Temperature was logged at 0.02 s intervals. Fig. 2 shows the substrate surface temperature over time with t = 0 s being the time when the gas jet was moved onto the substrate surface. The temperature reading reached 500 °C within 3 s and then became constant at 511 °C after 17 s.

The velocities and temperatures of particles exiting the cold spray nozzle were calculated using a 1d isentropic model. Details of the model have been provided in an earlier publication [23]. The Mach

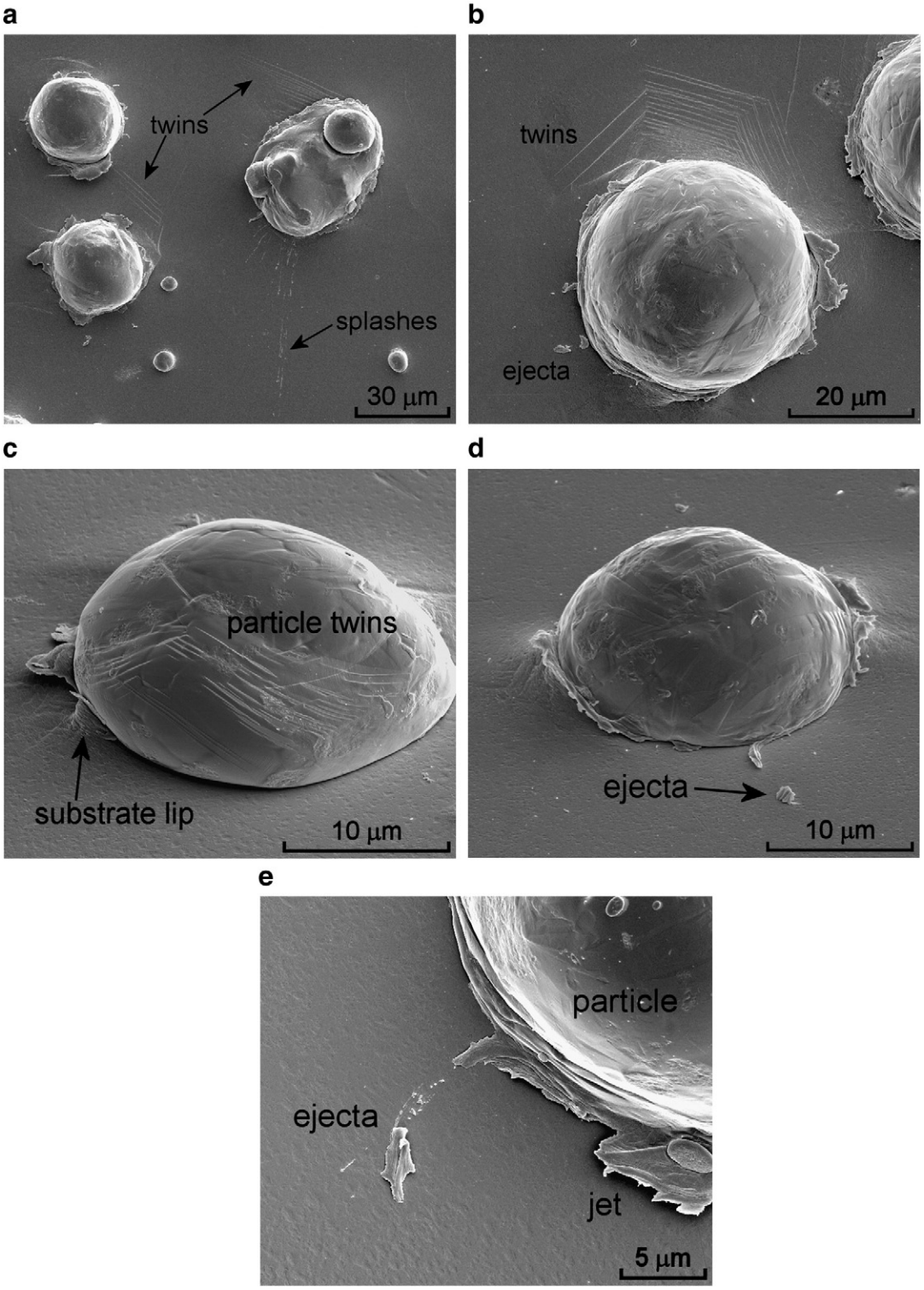

Fig. 3. Secondary electron images of adhered particles, deformation and jetting features. (a), (b), (e) top-down views, and (c), (d) views at 52° stage tilt.

number, M, of the gas phase at any distance through the nozzle was first found from the ratio of the local nozzle area, A, to the throat area A^*, Eq. (1).

$$\left(\frac{A}{A^*}\right)^2 = \frac{1}{M^2}\left[\frac{2}{\gamma+1}\left(1+\frac{\gamma-1}{2}M^2\right)\right]^{(\gamma+1)/(\gamma-1)} \quad (1)$$

where γ is the specific heat ratio.

Other local properties of the gas phase – temperature, pressure, density and velocity – are basic functions of M, γ and the stagnation conditions. Acceleration of a spherical particle of diameter d_p and density ρ_p within this flow field was then determined using Eq. (2) [24].

$$\frac{dv_p}{dt} = \frac{3C_D\rho_g}{4d_p\rho_p}\left(v_g - v_p\right)^2 \quad (2)$$

where ρ_g and v_g are the gas density and velocity, respectively, and C_D is the drag coefficient. C_D was calculated according to Henderson [25].

Particle heating/cooling followed Eq. (3).

$$\frac{dT_p}{dt} = \frac{6\lambda_g Nu}{c_{pp}\rho_p d_p^2}\left(T_g - T_p\right) \quad (3)$$

where λ_g is the gas thermal conductivity, Nu the Nusselt number, c_{pp} the particle specific heat, and T_p and T_g the particle and gas temperature, respectively.

Dissections of particles in the center of the spray area were performed using an FEI Helios NanoLab 600 Dual Beam Focused Ion Beam/Scanning Electron Microscope (FIB/SEM). Prior to FIB/SEM the samples were sputtered coated with iridium. All imaging of the surface and of the milled cross-sections was done on SEM mode at 5 kV. A 30 kV Ga^+ ion beam was used to mill rectangular trenches into the particle and surrounding substrate, until half of the particle was removed. For fast material removal, currents between 0.92 nA and 21.0 nA were employed. For the final cleaning steps closest to the particle centerline, the current was lowered to the range 93 pA–2.8 nA [26].

3. Results

3.1. External features of the adhered particles and surrounding substrate

Before milling any particles a general survey of the surface was made using SEM mode only.

Deformation twinning brought about characteristic surface relief patterns in both the substrate and particles. In the substrate adjacent to particles, groups of twins were commonly found, extending up to ~one particle diameter from the particle edge (Fig. 3a, b). FIB milling (Section 3.2) revealed that these were rows of long, straight twins, sometimes spaced as little as 100 nm apart. There were also other straight and lenticular twins below the surface or within the particle which did not intersect the surface.

From the external view, jetting caused by adiabatic shearing within the particle was clearly evident in most impacts. Larger particles generally displayed more prominent jets. On the other hand, substrate jetting appeared less common, although it may have been masked to some degree by the particle in top-down view. In more asymmetrical impacts substrate jetting was more likely on the side of the particle closer to the center of mass (i.e. closer to the highest point of the particle — Fig. 3c). Schmidt et al. modeled oblique impact of a Cu particle and found a more prominent 'lip' in the substrate ahead of the particle, and reduced jetting behind [27].

Material ejected from impacts was commonly found on the surface. There were two forms of ejecta. The first (Fig. 3b, d) was detached pieces of material, or 'chips', which had been thrown outwards, usually landing several micrometers away. They shared the same morphology as the plastically deformed material still attached to the particles in the jets. The second type of ejecta (Fig. 3a) was liquid splashes, which took the form of spheroidized droplets. Similar splashes have been seen in other studies of cold spray particle impact and are known to be associated with interfacial melting [15,17]. Fig. 3e shows a hybrid form — a plastically deformed chip, with skidding marks on the surface and molten splashes.

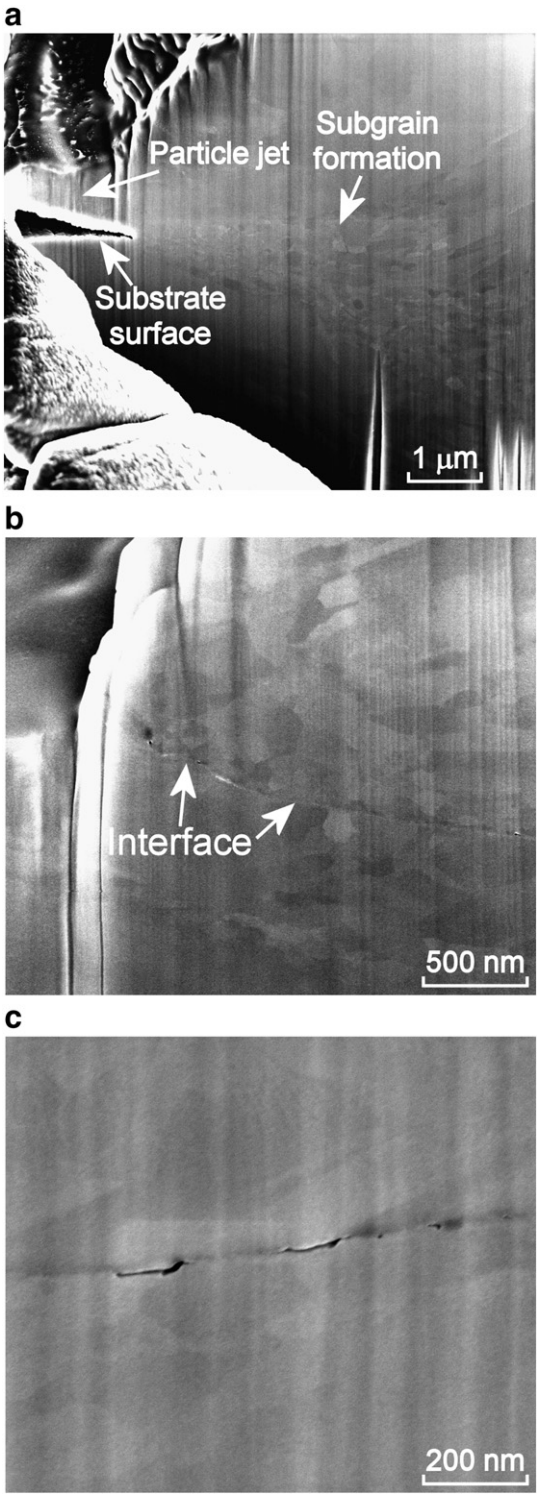

Fig. 4. High contrast secondary electron images of a section of the milled surface in (a) a 28.6 μm particle and (b) a 5.6 μm particle. (c) High magnification image showing a section of an interface with voids.

3.2. FIB milling to reveal the internal features of the adhered particles

A total of ten particles were milled using the FIB. All particles were chosen from the center of the spray area. Those with an irregular morphology or which had been impacted by other particles were excluded from the study (e.g. particle in top-right of Fig. 3a).

Following the final milling step at low beam current some microstructure could be made out in secondary electron mode due to crystallographic contrast (Fig. 4). This technique has been shown to be useful in copper [28]. A complete discussion of microstructural evolution is outside the scope of this paper. However, it can be generally stated that the microstructure was highly complicated and non-homogeneous, resulting from the steep gradient in thermomechanical conditions though the particle, the limited slip systems available in hcp titanium, and the complex relationship between twinning and dislocation slip [29]. Strains at the interface are much higher than those in the middle of the particle [22]. In the FIB/SEM images there was a concentration of fine (<100 nm) grains near the interface. Similar broad regions of intense microstructural refinement have been observed by transmission electron microscopy of deposits made from hydride–dehydride Ti powder using the same accelerating gas parameters [2]. Since identically-sized grains were found on either side of the interface

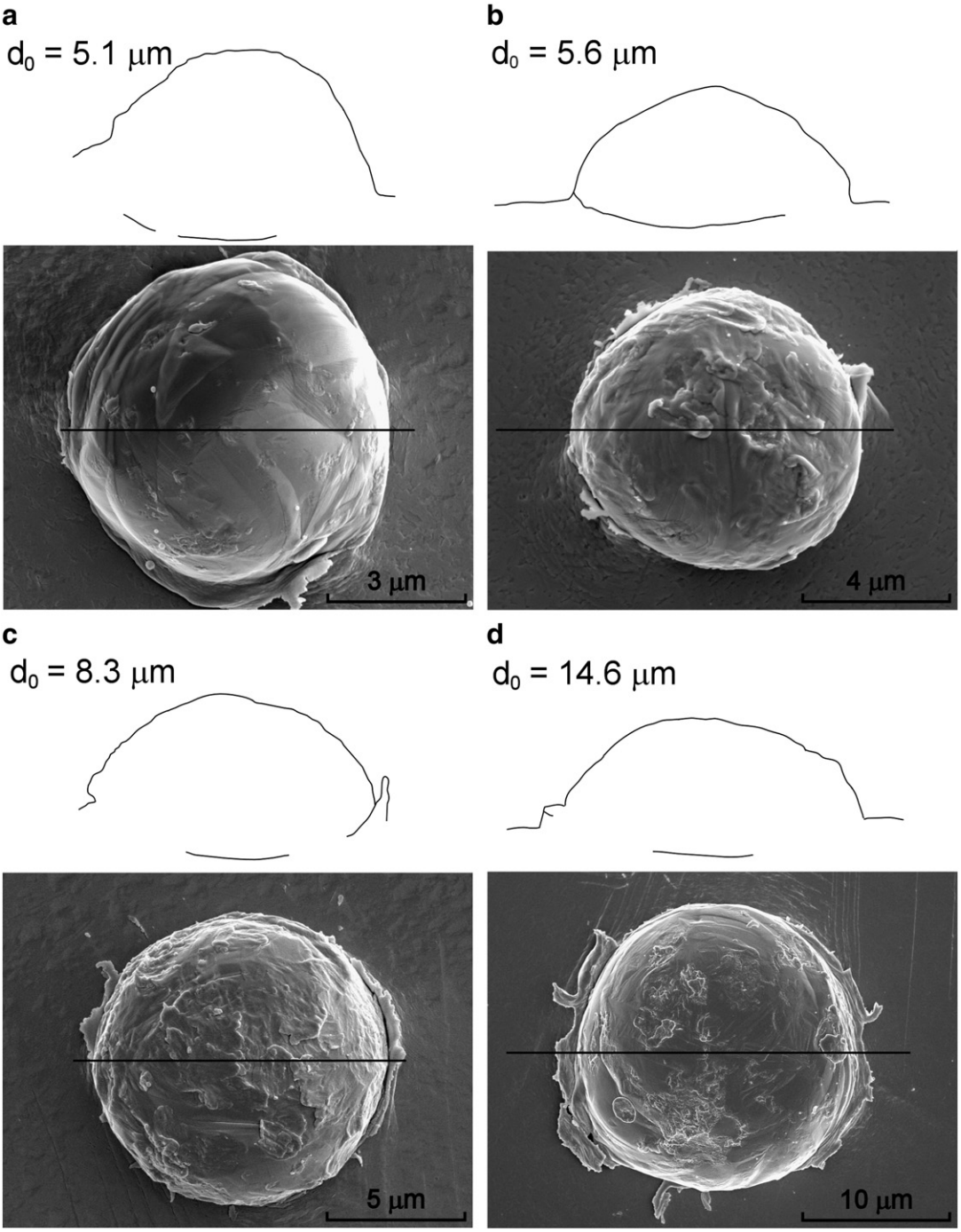

Fig. 5. Milled particles; SEM top-down view, particle outline determined from FIB cross-section and calculated original particle diameter (d_0). Trenches were milled from the bottom of the SEM images upwards, until the horizontal halfway line was reached.

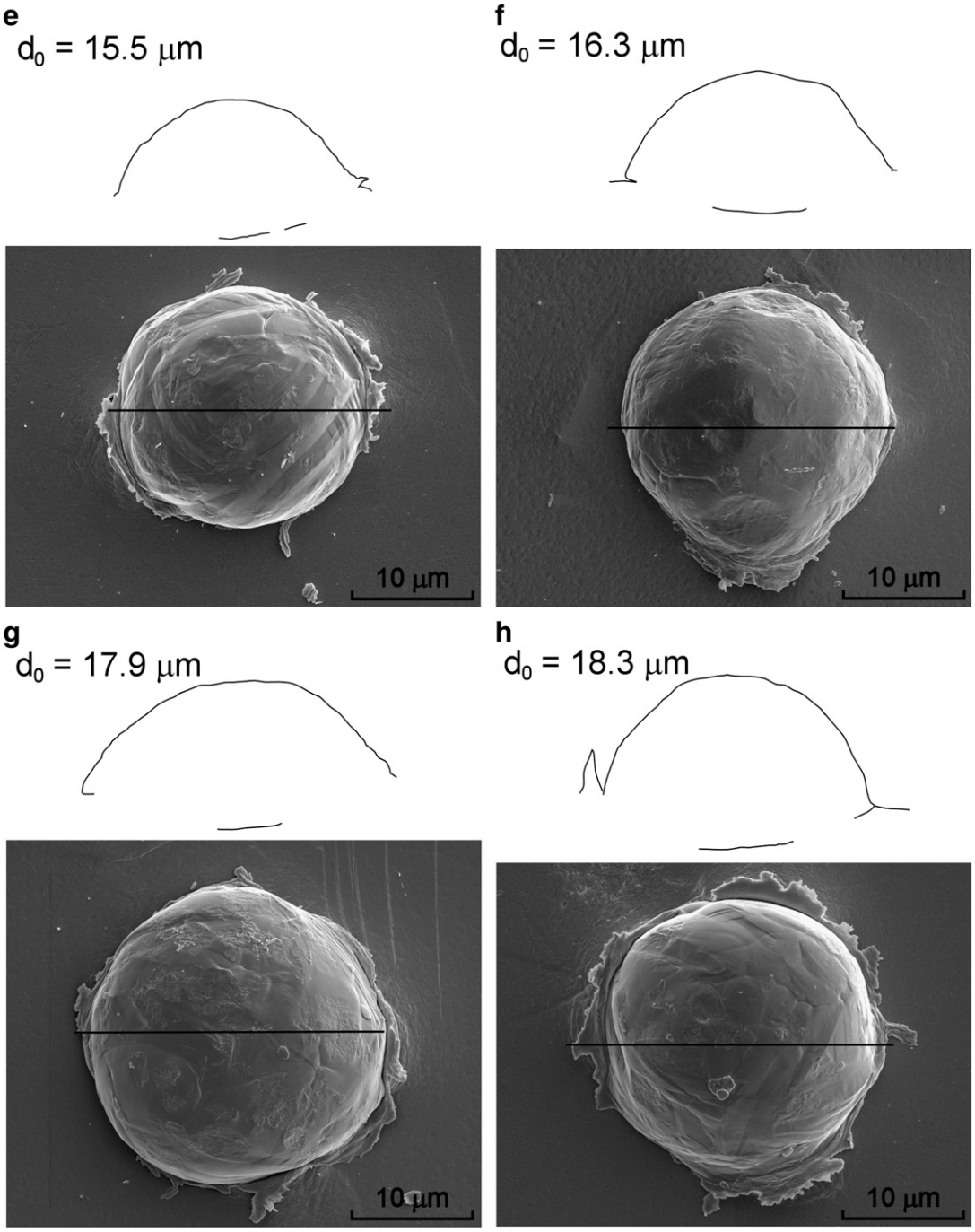

Fig. 5 (*continued*).

in the titanium of the substrate and of the particle, it was clear that this level of microstructural refinement was a general feature of the response of this material to the local deformation conditions.

A notable outcome of the FIB study was that some sections of the particle–substrate interface were well delineated (e.g. Fig. 4b, c), while in other places the interface could not be found. In the former case it was marked by a series of voids or gaps, resolvable at high magnification (Fig. 4c). However, in Fig. 4a (from 28.6 μm particle) the boundary between particle and substrate could not be determined due to an apparent 'melding' of the interface. That this occurred in the peripheral region near a well-formed jet was not a random occurrence, as will be proven by a full survey of the particle cross-sections.

Fig. 5 contains the full set of ten milled particles, showing the overall shape of the deformed particle/substrate system and the sections of the interface that remained unmelded. For each particle the following is presented; (a) a top-down, secondary electron image of the whole particle before milling, and (b) an outline of the particle in cross-section determined from FIB milling. The location of the particle–substrate interface was drawn only where it could be clearly identified, as described above. Since the ion and electron columns were at an angle of 52° to each other, the ion milled face was always tilted with respect to the electron column. Therefore the outlines in Fig. 5 were stretched vertically by a factor of $\sin^{-1}(52°)$ in order to correct for stage tilt.

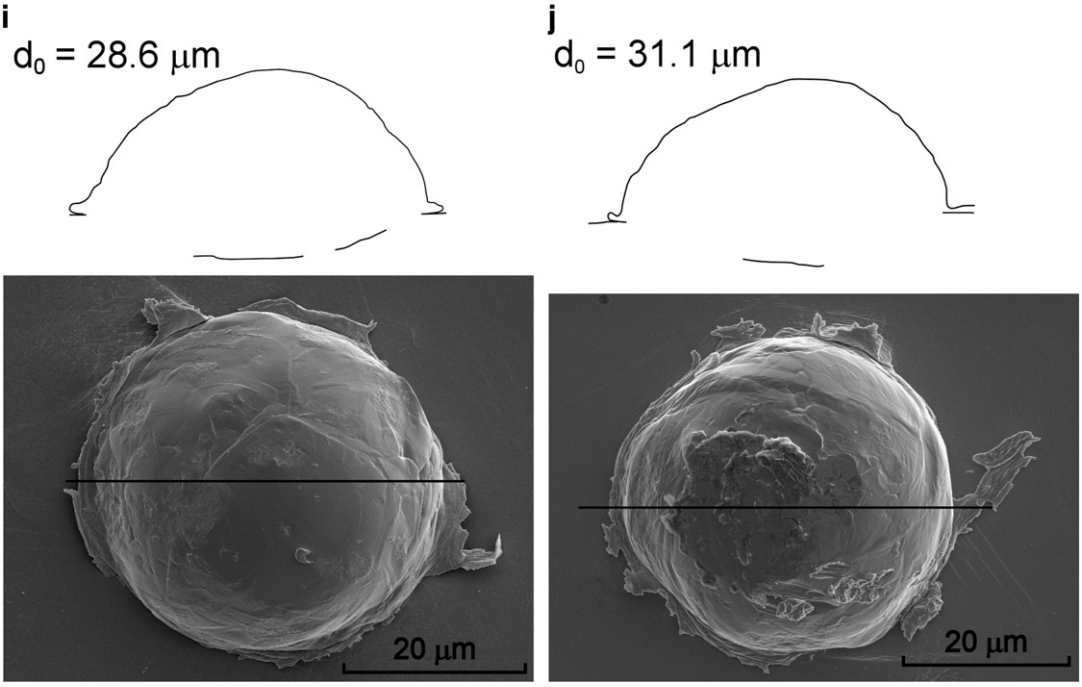

Fig. 5 (*continued*).

The particle diameter prior to impact, d_0, could be calculated from the cross-section by the method of Riemann sum [30]. n measurements of the particle width, $w_{i,}$ were made at regular intervals, $\Delta h_{i,}$ down through the particle to the base. For the purpose of this calculation, interpolation was used to connect up the known sections of the interface. Volume was then calculated by assuming rotational symmetry about the vertical axis:

$$V = \sum_{i=1}^{n} \frac{\pi w_i^2}{4} \Delta h_i. \quad (4)$$

From conservation of volume, d_0 of an initially spherical particle is given by

$$d_0 = \sqrt[3]{\frac{6V}{\pi}}. \quad (5)$$

Two quantitative measures were made from the line profiles in Fig. 5 — flattening ratio and void length ratio.

Flattening ratio, ε, is a commonly-used measure of shape distortion in impacts of spherical particles [30]. It is defined as;

$$\varepsilon = \frac{d_0 - h}{d_0} \quad (6)$$

where h is the height of the deformed particle after impact.

The flattening ratios of the dissected particles are summarized in Fig. 6a. The particles were grouped into three size brackets; small (d_0 = 5–8 μm), medium (15–18 μm), and large (29–31 μm), and an average ε and standard deviation were calculated for each group.

The same particle groupings were used for a study of the particle–substrate interfaces, in Fig. 6b and Fig. 6c. Fig. 6b shows the total interface length containing voids, in other words the summed length of the lines underneath each particle in Fig. 5. For the measurements, curved lines were fitted by a series of shorter straight line segments. Again, an average value was calculated for each particle size range.

Also of interest was the extent of interfacial melding. The fully melded sections of the interface were obtained by interpolating between the void-containing sections. Fig. 6c gives the fraction of the total interface length that was melded.

4. Discussion

It was immediately evident from the FIB cross-sections that adhesion of the cold sprayed titanium particles did not require intimate bonding along the entire interface, and in fact that this was never achieved. This is despite the fact that the deposition conditions were favorable for particle retention, and empty impact craters were difficult to find. Thus it seems that a coating built up by further particle impact would have retained a high proportion of internal surfaces containing voids.

In all 10 dissected particles, the fraction of the interface that was 'melded' did not ever exceed 77% of the total interpolated interface length. On the other hand, the minimum melded fraction was 26% (in the 5.6 μm particle). Area analysis (as opposed to linear fractions) may have been performed by a quasi-three-dimensional process, involving a series of milling steps from one side of the particle through to the other. However, considering the size of the particles and due to the fact that each section of the interface needed to be examined closely, this sort of procedure would have proven very time consuming.

Strings of voids such as those in Fig. 4c show that the particle and substrate topologies did not match on a nanometer level. Depending on the impact conditions, rebound forces may widen the gap out to a thick crack below the particle [31,32]. Voids were consistently found at the base of the particle, but usually tended to disappear at the peripheries (although not always, e.g. Fig. 4b), depending on particle size, symmetry effects (see below) and particle and substrate jetting. When the interfaces were divided into 3 equal sections it was found that on average, 81 ± 4% of the bottom 3rd surrounding the south pole was void-containing, compared with 21 ± 5% in the left and right peripheral sections. Thus, it is proposed that nanoscale contact was produced by viscous-like flow in the adiabatic shear zones. In the south pole region high compressive stress alone was insufficient to fill the volume between asperities. In the shear zones however, it was aided by softening up to the melting point.

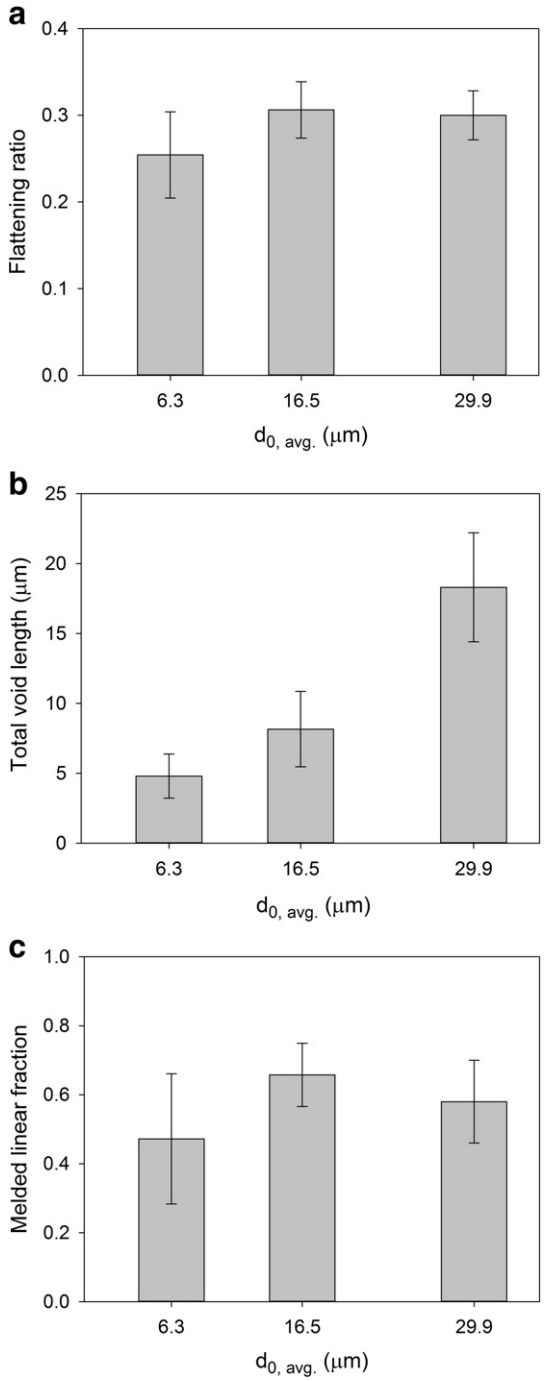

Fig. 6. (a) Flattening ratio, ε, (b) void-containing length of the interface and (c) melded fraction of the total interface length — average values for 3 different particle sizes, determined from the line profiles in Fig. 5. Error bars indicate standard deviation.

It has been established that the maximum gas temperature in the system was 600 °C, while the substrate surface reached a constant 511 °C. When compared to the melting point of titanium, 1660 °C, and the evidence of molten droplet formation, this illustrates the extent of interfacial heating. Strain localization is intensified in titanium by its low thermal conductivity (21.9 $Wm^{-1}\ K^{-1}$) which hampers heat withdrawal from shear zones [2].

There was considerable variation in the morphology of the titanium splats and in the occurrence of jetting (Fig. 5). In fact, most impacts could not be described as highly symmetrical. However, from a survey of the particles no systematic directionality could be found, i.e. they were not aligned with respect to each other. Since the study was restricted to the center of the spray area, the possibility of off-normal impacts can be eliminated (unless the majority of particles follow bowed trajectories, returning back to the center line at 30 mm from the nozzle exit). Rather it appears that on this scale, microstructural effects may play a large role. For instance, the grain size of the substrate was comparable to the 'medium'-sized particle diameter (Fig. 6). Surface relief from twins in the substrate were frequently only found on one side of the particle (Fig. 3b).

A further effect is that while gas atomized metal powders generally possess excellent sphericity and smoothness, there is always at some level a degree of roughness, lumpiness or other imperfections (Fig. 1). As mentioned an average aspect ratio of 1.12 was measured for the Ti powder. Since adiabatic shear is essentially an instability phenomenon, it may be disproportionately influenced by these asymmetries.

Taking these considerations into account it is unsurprising that the standard deviation in the quantitative measurements (error bars, Fig. 6) was rather high. Nevertheless, the following overall trends were found. The total length of interface containing voids (Fig. 6b) increased with increasing particle size. The longest single sections of interface which were not melded were 10.0 and 12.3 μm, found under the largest and second-largest particles, respectively. This was clearly an effect of scaling, i.e. a 12.3 μm-wide defect could not possibly fit beneath only one 6.3 μm particle. Nevertheless, long sections of void-containing interface may be a concern where mechanical properties of the deposit are concerned.

When melding was expressed as a fraction of the total interface length (Fig. 6c) it became apparent that a higher proportion of the interface was melded for particles in the 16.5 μm group. The largest particles (29.9 μm group) suffered lower acceleration through the cold spray nozzle (Fig. 7). Smaller particles (6.3 μm group) exhibited lower flattening ratios (compare Fig. 6a and c) and less-pronounced jetting due to a number of factors.

Although smaller particles are easier to accelerate through the de Laval nozzle and may achieve higher velocities than larger particles, they also suffer greater deceleration through the bow shock zone in front of the substrate [33]. Thus the velocities of a 6.3 μm particle at the point of impact may have been lower than indicated in Fig. 7. Furthermore, due to faster cooling in the nozzle diverging section, there is a drop in temperature for smaller particles exiting the Laval nozzle (Fig. 7) and consequently less improvement in deformability due to thermal softening. As pointed out by Schmidt et al. the formation of shear instabilities may be hindered in small particles by the shorter impact durations which increase the strain-rate hardening effect [12].

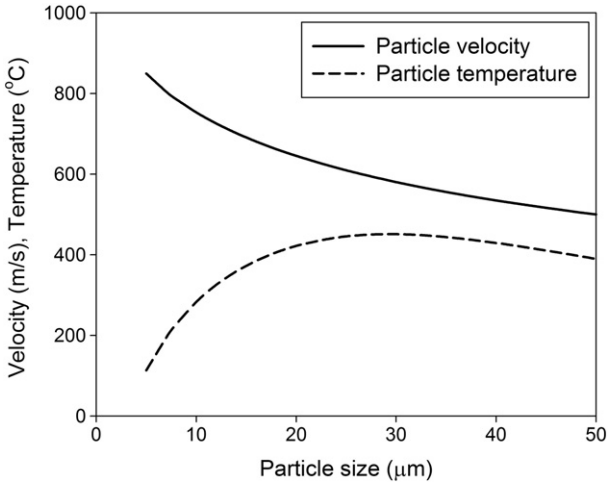

Fig. 7. Predicted particle velocities and temperatures at the nozzle exit.

Thus, for maximal fraction of melded interface an optimum particle size range appears to exist.

Kim et al. investigated titanium impacts onto steel surfaces by the higher temperature warm spray process. They did not find any correlation between the bonded fraction of the interface and particle size. However, given the much greater overall level of deformation, the results may not be directly comparable with those in the current study [21].

The relevance of the current study to a 'real' coating scenario deserves some comment. Generally, cold spray coating is not static, but requires relatively rapid movement of the nozzle and/or workpiece, i.e. typically tens to hundreds of millimeters per second, although with rotation of large, cylindrical workpieces linear surface speeds are in the m/s range. This means that there is less time for heat transfer from the gas jet to the surface prior to arrival of the first particles, although the surface temperature will rise with repeated coating passes. On balance however, rather than the surface temperature being higher than the particle temperature, the reverse is probably more likely in practice, which would tend to limit substrate deformation and favor particle jetting.

Recent developments in cold spray gun design have seen a push towards higher gas temperatures and pressures with the aim of improving particle acceleration, particularly for less ductile metals such as titanium [34]. Higher gas temperatures also mean increased heat transfer to the particles and substrate. In the current static experiments the gas temperature was limited to 600 °C to avoid oxidation of the sample surface. However, with commercial systems now able to achieve stagnation conditions of 800–1100 °C and 5 MPa, and with improvements in nozzle design, greater particle deformation could be expected, which would influence the ratio of melded to void-containing interfaces.

5. Conclusion

It has been shown that at the interface between cold sprayed Ti particles and a Ti surface, voids are present due to nanometer-scale mismatch in surface topologies. These voids were eliminated over a linear fraction of 26–77% of the interface by plastic flow during impact deformation, making the interface appear 'melded'. Void closure was more likely at the particle peripheries, and rarely achieved at the particle base. Thus, void closure was associated with adiabatic shearing, which occurred at the peripheries, was sufficiently intense to raise the temperature of the interfacial layers to melting point, and caused a viscous-like flow of material.

Acknowledgments

The authors are grateful to Andrew Urban from CSIRO Process Science and Engineering for his assistance with temperature data collection. This work was performed in part at the Melbourne Centre for Nanofabrication. Financial support for this research was provided by CSIRO's Future Manufacturing Flagship.

References

[1] A.P. Alkhimov, V.F. Kosarev, A.N. Papyrin, Sov. Phys. Dokl. 35 (1990) 1047–1049 (Transl. American Institute of Physics, 1991).
[2] P.C. King, M. Jahedi, in: B. Marple, A. Agarwal, M. Hyland, Y.-C. Lau, C.-J. Li, R.S. Lima, G. Montavon (Eds.), Thermal Spray: Global Solutions for Future Application, Springer, Singapore, 2010.
[3] S.H. Zahiri, C.L. Antonio, M. Jahedi, J. Mater. Process. Technol. 209 (2009) 922–929.
[4] R.E. Blose, B.H. Walker, R.M. Walker, S.H. Froes, Met. Powder Rep. 61 (2006) 30–37.
[5] D. Goldbaum, J. Ajaja, R.R. Chromik, W. Wong, S. Yue, E. Irissou, J.-G. Legoux, Mater. Sci. Eng. A 530 (2011) 253–265.
[6] J. Karthikeyan, C.M. Kay, J. Lindeman, R.S. Lima, in: C.C. Berndt (Ed.), Thermal Spray Surface Engineering via Applied Research, Proceedings: 1st International Thermal Spray Conference (ITSC 2000), ASM International, Materials Park, OH, Montreal, Canada, 2000, pp. 255–262.
[7] W. Wong, A. Rezaeian, E. Irissou, J.-G. Legoux, S. Yue, Adv. Mater. Res. 89–91 (2010) 639–644.
[8] T. Marrocco, D.G. McCartney, P.H. Shipway, A.J. Sturgeon, J. Therm. Spray Technol. 15 (2006) 263–272.
[9] R.S. Lima, A. Kucuk, C.C. Berndt, J. Karthikeyan, C.M. Kay, J. Lindeman, J. Mater. Sci. Lett. 21 (2002) 1687–1689.
[10] M. Grujicic, C.L. Zhao, W.S. DeRosset, D. Helfritch, Mater. Des. 25 (2004) 681–688.
[11] H. Assadi, F. Gartner, T. Stoltenhoff, H. Kreye, Acta Mater. 51 (2003) 4379–4394.
[12] T. Schmidt, F. Gartner, H. Assadi, H. Kreye, Acta Mater. 54 (2006) 729–742.
[13] M. Grujicic, J.R. Saylor, D.E. Beasley, W.S. DeRosset, D. Helfritch, Appl. Surf. Sci. 219 (2003) 211–227.
[14] R.C. Dykhuizen, M.F. Smith, D.L. Gilmore, R.A. Neiser, X. Jiang, S. Sampath, J. Therm. Spray Technol. 8 (1999) 559–564.
[15] P.C. King, S.H. Zahiri, M.H. Jahedi, Acta Mater. 56 (2008) 5617–5626.
[16] G. Bae, S. Kumar, S. Yoon, K. Kang, H. Na, H.-J. Kim, C. Lee, Acta Mater. 57 (2009) 5654–5666.
[17] P.C. King, G. Bae, S. Zahiri, M. Jahedi, C. Lee, J. Therm. Spray Technol. 19 (2010) 620–634.
[18] S. Barradas, V. Guipont, R. Molins, M. Jeandin, M. Arrigoni, M. Boustie, C. Bolis, L. Berthe, M. Ducos, J. Therm. Spray Technol. 16 (2007) 475–479.
[19] S. Guetta, M. Berger, F. Borit, V. Guipont, M. Jeandin, M. Boustie, Y. Ichikawa, K. Sakaguchi, K. Ogawa, J. Therm. Spray Technol. 18 (2009) 331–342.
[20] J. Wu, H. Fang, H. Kim, C. Lee, Mater. Sci. Eng. A 417 (2006) 114–119.
[21] K. Kim, M. Watanabe, S. Kuroda, J. Therm. Spray Technol. 18 (2009) 490–499.
[22] D. Goldbaum, R. Chromik, S. Yue, E. Irissou, J.-G. Legoux, J. Therm. Spray Technol. 20 (2011) 486–496.
[23] P.C. King, S. Zahiri, M. Jahedi, J. Friend, Surf. Coat. Technol. 205 (2010) 2016–2022.
[24] R.C. Dykhuizen, M.F. Smith, J. Therm. Spray Technol. 7 (1998) 205–212.
[25] C.B. Henderson, AIAA J. 14 (1976) 707–708.
[26] M.W. Phaneuf, Micron 30 (1999) 277–288.
[27] T. Schmidt, H. Assadi, F. Gärtner, H. Richter, T. Stoltenhoff, H. Kreye, T. Klassen, J. Therm. Spray Technol. 18 (2009) 794–808.
[28] P.C. King, S.H. Zahiri, M. Jahedi, Metall. Mater. Trans. A 40 (2009) 2115–2123.
[29] Y.B. Chun, S.H. Yu, S.L. Semiatin, S.K. Hwang, Mater. Sci. Eng. A 398 (2005) 209–219.
[30] P.C. King, M. Jahedi, Appl. Surf. Sci. 256 (2010) 1735–1738.
[31] K. Kim, M. Watanabe, S. Kuroda, Surf. Coat. Technol. 204 (2010) 2175–2180.
[32] D. Goldbaum, J. Shockley, R. Chromik, A. Rezaeian, S. Yue, J.-G. Legoux, E. Irissou, J. Therm. Spray Technol. 21 (2012) 288–303.
[33] R.C. Dykhuizen, R.A. Neiser, in: C. Moreau, B. Marple (Eds.), Thermal Spray 2003: Advancing the Science and Applying the Technology, ASM International, Materials Park, OH, Orlando, FL, 2003.
[34] W. Wong, E. Irissou, P. Vo, M. Sone, F. Bernier, J.G. Legoux, H. Fukanuma, S. Yue, J. Therm. Spray Technol. 22 (2013) 413–421.